

SUPERCONDUCTORS

Unified understanding of superconductivity and Mott transition in alkali-doped fullerenes from first principles

Yusuke Nomura,^{1*} Shiro Sakai,² Massimo Capone,³ Ryotaro Arita^{2,4}

Alkali-doped fullerenes A_3C_{60} ($A = K, Rb, Cs$) are surprising materials where conventional phonon-mediated superconductivity and unconventional Mott physics meet, leading to a remarkable phase diagram as a function of volume per C_{60} molecule. We address these materials with a state-of-the-art calculation, where we construct a realistic low-energy model from first principles without using a priori information other than the crystal structure and solve it with an accurate many-body theory. Remarkably, our scheme comprehensively reproduces the experimental phase diagram including the low-spin Mott-insulating phase next to the superconducting phase. More remarkably, the critical temperatures T_c 's calculated from first principles quantitatively reproduce the experimental values. The driving force behind the surprising phase diagram of A_3C_{60} is a subtle competition between Hund's coupling and Jahn-Teller phonons, which leads to an effectively inverted Hund's coupling. Our results establish that the fullerenes are the first members of a novel class of molecular superconductors in which the multiorbital electronic correlations and phonons cooperate to reach high T_c s -wave superconductivity.

INTRODUCTION

Alkali-doped fullerenes are unique exotic s -wave superconductors with maximum critical temperature $T_c \sim 40$ K, which is extremely high for the modest width of about 0.5 eV of the bands relevant to superconductivity (1–9). Although the evidence for a phononic pairing mechanism is robust and may suggest a conventional explanation for the superconductivity in these materials (2), the experimental observation of a Mott-insulating phase next to the superconducting phase in Cs_3C_{60} changes the perspective because the same strong correlations responsible for the Mott state are also likely to influence the superconducting state (3–9). This raises the fundamental question of why s -wave superconductivity, which is induced by some attractive interaction, is so resilient to (or even enhanced by) the strong repulsive interactions (2). The fingerprints of phonons observed in the Mott-insulating phase, such as the low-spin state (4–9) and the dynamical Jahn-Teller effect (10), confirm a nontrivial cooperation between the electron correlations and the electron-phonon interactions.

A variety of scenarios have been proposed to explain the superconductivity (2, 11–21). However, even the most successful theories include some adjustable parameter and/or neglect, for example, the realistic band structure, the intermolecular Coulomb interactions, and Hund's coupling. These assumptions have prevented these theories from being conclusive on the superconducting mechanism, which arises from a subtle energy balance between the Coulomb and the electron-phonon interactions in a multiorbital system. Therefore, to pin down the pairing mechanism, a nonempirical analysis is indispensable: If fully ab initio calculations quantitatively reproduced the phase dia-

gram and T_c , they would provide precious microscopic information to identify unambiguously the superconducting mechanism, opening the path toward a predictive theory of superconductivity in correlated molecular materials.

Here, we carry out such nonempirical analysis using a combination of density functional theory (DFT) and dynamical mean-field theory (DMFT), an approach that accurately describes the properties of many correlated materials (22). DMFT is particularly accurate for compounds with short-range interactions and a large coordination number z , such as A_3C_{60} , a highly symmetric three-dimensional system with $z = 12$.

RESULTS

Theoretical phase diagram and comparison with experiments

In Fig. 1, we show the band structure obtained within DFT for face-centered cubic (fcc) Cs_3C_{60} . Because the t_{1u} bands crossing the Fermi level are well isolated from the other bands, we construct a lattice Hamiltonian consisting of the t_{1u} electron and phonon degrees of freedom. The Hamiltonian is defined in the most general form:

$$\mathcal{H} = \sum_{ij\mathbf{k}\sigma} \mathcal{H}_{ij}^{(0)}(\mathbf{k}) c_{i\mathbf{k}}^{\sigma\dagger} c_{j\mathbf{k}}^{\sigma} + \sum_{\mathbf{q}\mathbf{k}\mathbf{k}'} \sum_{ijj'\sigma\sigma'} U_{ij,i'j'}(\mathbf{q}) c_{i\mathbf{k}+\mathbf{q}}^{\sigma\dagger} c_{j\mathbf{k}'}^{\sigma\dagger} c_{i'\mathbf{k}'+\mathbf{q}}^{\sigma'} c_{j'\mathbf{k}}^{\sigma'} + \sum_{ijk\sigma q\nu} g_{ij}^{\nu}(\mathbf{k}, \mathbf{q}) c_{i\mathbf{k}+\mathbf{q}}^{\sigma\dagger} c_{j\mathbf{k}}^{\sigma} (b_{q\nu} + b_{-q\nu}^{\dagger}) + \sum_{q\nu} \omega_{q\nu} b_{q\nu}^{\dagger} b_{q\nu}, \quad (1)$$

on the fcc lattice, where each site represents a C_{60} molecule. $\mathcal{H}^{(0)}$, U , g , and ω are the electron one-body Hamiltonian, Coulomb interaction, electron-phonon coupling, and phonon frequency, respectively. They all have indices of the Wannier orbitals i, j, i', j' , spin σ, σ' , momentum \mathbf{k}, \mathbf{q} , and the phonons also have a branch index ν . We construct maximally localized Wannier orbitals (23) as the basis for making the hopping and interaction parameters as short-ranged as possible. We determine all of the above parameters by state-of-the-art ab initio techniques (Materials and Methods). In particular, the recently developed constrained density-functional perturbation theory (cDFPT) (24) has

¹Department of Applied Physics, University of Tokyo, Hongo, Bunkyo-ku, Tokyo 113-8656, Japan. ²Center for Emergent Matter Science (CEMS), RIKEN, 2-1, Hirosawa, Wako, Saitama 351-0198, Japan. ³International School for Advanced Studies (SISSA) and Consiglio Nazionale delle Ricerche—Istituto Officina dei Materiali (CNR-IOM) Democritos National Simulation Center, Via Bonomea 265, I-34136 Trieste, Italy. ⁴Japan Science and Technology Agency (JST) ERATO Isobe Degenerate π -Integration Project, Advanced Institute for Materials Research (AIMR), Tohoku University, 2-1-1 Katahira, Aoba-ku, Sendai 980-8577, Japan.

*Corresponding author. E-mail: yusuke.nomura@riken.jp

enabled calculations of the phonon-related terms (g_{ij}^v and ω_{qv}), where the effects of the high-energy bands are incorporated into the parameter values. To solve the ab initio model, we used the extended DMFT (E-DMFT) (22), which combines the ability of DMFT to treat local interactions with the inclusion of nonlocal terms. To study the superconductivity, we introduced the anomalous Green's function, whose integral over frequency gives superconducting order parameter, into the E-DMFT equations.

Figure 2A shows the theoretical phase diagram as a function of temperature T and volume per C_{60}^{3-} anion ($V_{C_{60}^{3-}}$). As a function of T and $V_{C_{60}^{3-}}$, we find a paramagnetic metal, a paramagnetic Mott insulator, and the s -wave superconducting phase where two electrons in

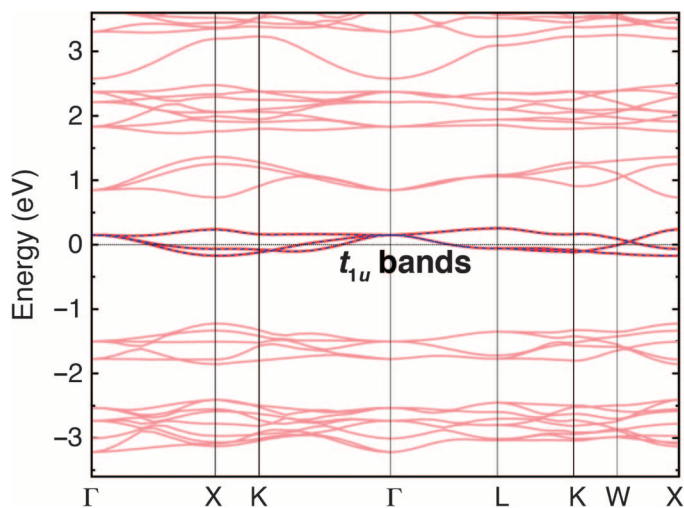


Fig. 1. Band structure of fcc Cs_3C_{60} with $V_{C_{60}^{3-}} = 762 \text{ \AA}^3$. The blue dotted curves represent the Wannier-interpolated band dispersion calculated from $\mathcal{H}_{ij}^{(0)}$ in Eq. 1.

the same orbital form the Cooper pairs. The three phases are characterized by a finite spectral weight at the Fermi level, a Mott gap, and nonzero anomalous Green's function and order parameter, respectively. The metal-insulator transition is of the first order below 80 K, and a direct first-order superconductor-insulator transition takes place around $V_{C_{60}^{3-}} = 780 \text{ \AA}^3$ at low temperature. Between the blue solid line $V_{c2}(T)$ and the black dotted line $V_{c1}(T)$, we find both a metallic and an insulating solution. The first-order transition line $V_c(T)$, where the free energies of the two solutions cross, is expected to be close to $V_{c2}(T)$ at low temperature as in the pure multiorbital Hubbard model (25).

In Fig. 2B, we reproduce the experimental phase diagram (9) for fcc A_3C_{60} systems to highlight the impressive agreement with our calculations. In particular, the maximum T_c of $\sim 28 \text{ K}$ in theory is comparable to that of the experiment $\sim 35 \text{ K}$ (5, 9). The critical volumes and the slope of the metal-insulator transition line are also consistent with the experiment. It is remarkable that our fully ab initio calculation, without any empirical parameters, reproduces quantitatively the experimental phase diagram including the unconventional superconductivity and the Mott insulator.

Unusual intramolecular interactions as a key for unconventional physics

The success of our theory in reproducing the experimental phase diagram demonstrates the reliability of the whole scheme including the estimates of the interaction parameters. We are therefore in a position to disentangle the crucial ingredients leading to the proximity of the s -wave superconductivity and a Mott insulator in the same diagram. The key quantities are the effective intramolecular interactions (intraorbital and interorbital density-density interactions $U_{\text{eff}} = U + U_V + U_{\text{ph}}$ and $U'_{\text{eff}} = U' + U'_V + U'_{\text{ph}}$, and exchange term $J_{\text{eff}} = J + J_{\text{ph}}$) between the t_{1u} electrons, which are used as input interaction parameters for the E-DMFT calculation. Here, U , U' , and J are the intramolecular

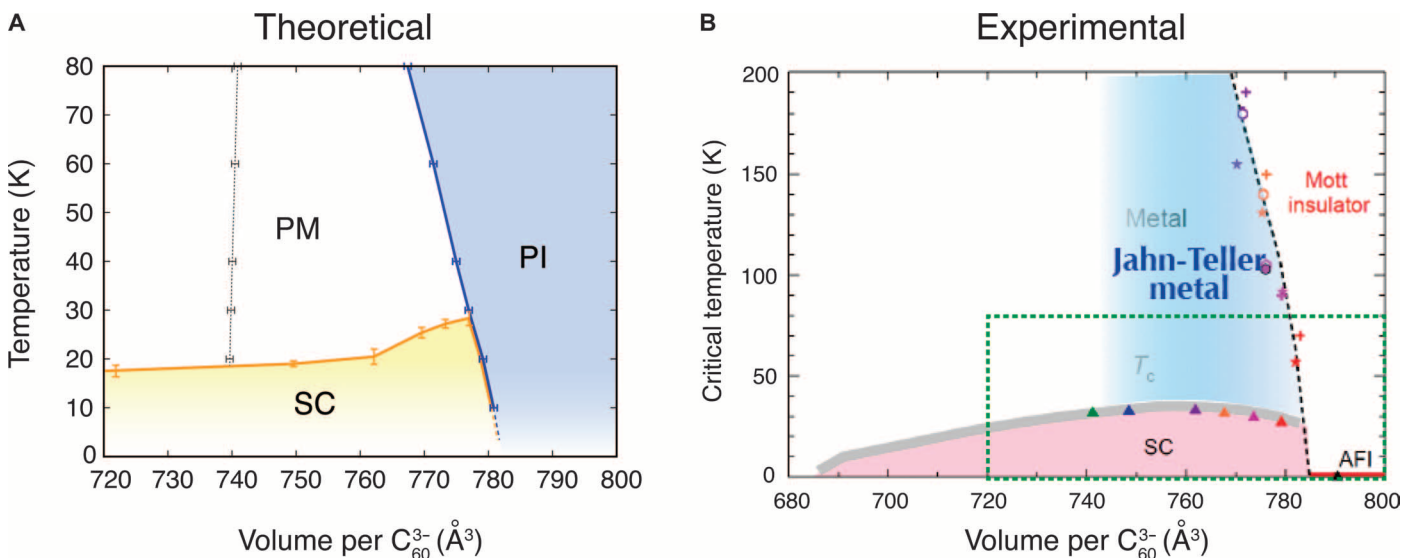


Fig. 2. Theoretical and experimental phase diagrams. (A) Phase diagram as a function of volume per C_{60} molecule and temperature, obtained with the DFT + E-DMFT. PM, PI, and SC denote the paramagnetic metal, the paramagnetic insulator, and the superconducting phase, respectively. Metallic and insulating E-DMFT solutions coexist between the blue solid line $V_{c2}(T)$ and the black dotted line $V_{c1}(T)$. The error bars for T_c originate from the statistical errors in the superconducting order parameters calculated with the quantum Monte Carlo method (see Section E in the Supplementary Materials for details). The error bars for $V_{c1}(T)$ and $V_{c2}(T)$ are half the interval of the volume grid in the calculation. (B) For comparison, the experimental phase diagram [adapted by Y. Kasahara from Figure 6 in Zadik *et al.* (9)] is shown, where the region depicted in (A) corresponds to the area surrounded by the green dotted lines. AFI denotes the antiferromagnetic insulator.

Coulomb interactions screened by the high-energy electrons, whereas $U_V = U'_V$ and $J_V = 0$ (U_{ph} , U'_{ph} , and J_{ph}) represent dynamical screening contributions from the intermolecular Coulomb (electron-phonon) interactions. These dynamical screening effects make the effective interactions dependent on electron's frequency ω .

The solid curves in Fig. 3 show $U_{eff}(\omega)$ and $U'_{eff}(\omega)$, where we find $U'_{eff}(\omega) > U_{eff}(\omega)$ up to $\omega \sim 0.2$ eV except a narrow region around $\omega = 0.1$ eV. This remarkable inversion of the low-energy interactions is associated with the negative value of $J_{eff}(0)$ discussed below because the relation $U'_{eff}(\omega) \sim U_{eff}(\omega) - 2J_{eff}(\omega)$ holds. As is apparent from $U > U'$ and $U + U_V > U' + U'_V$ (plotted by dotted and dashed curves in Fig. 3), it is the phonon contribution (U_{ph} , U'_{ph} , and J_{ph}) that causes the inversion. In fact, $U_{ph}(\omega)$ and $U'_{ph}(\omega)$ have strongly ω -dependent structures for $\omega \lesssim 0.2$ eV because of the intramolecular Jahn-Teller phonons with the frequencies up to ~ 0.2 eV (2), which are comparable to the t_{1u} bandwidth ~ 0.5 eV.

Table 1 shows the static ($\omega = 0$) values of the phonon-mediated interactions for various A_3C_{60} compounds. For all the interactions, the phonon contribution has an opposite sign with respect to U , U' , and J . Whereas $|U_{ph}(0)|$ and $|U'_{ph}(0)|$ are much smaller than U and $U' \sim 1$ eV, $|J_{ph}(0)| \sim 51$ meV is remarkably larger than that of the positive Hund's coupling $J \sim 34$ meV (26). As a result, an effectively negative exchange interaction $J_{eff}(0) = J + J_{ph}(0) \sim -17$ meV is realized. The unusual sign inversion of the exchange interaction (17, 18, 27, 28) results from the molecular nature of the localized orbitals, which yields a small J , combined with a strong coupling between the Jahn-Teller phonons and t_{1u} electrons (2), which enhances $|J_{ph}(0)|$.

Microscopic mechanism of superconductivity

We find, through a detailed analysis (Section F in the Supplementary Materials), that the unusual multiorbital interactions indeed drives the

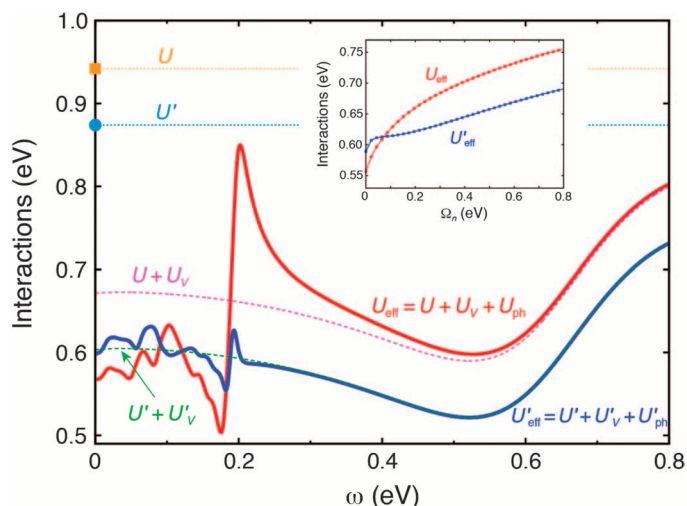


Fig. 3. Frequency dependence of effective onsite interactions. The effective intra- and interorbital interactions ($U_{eff} = U + U_V + U_{ph}$ and $U'_{eff} = U' + U'_V + U'_{ph}$, respectively) consist of the constrained random-phase approximation (cRPA) onsite Coulomb repulsion (U , U'), the dynamical screening from the off-site interactions ($U_V = U'_V$), and the phonon-mediated interactions (U_{ph} , U'_{ph}). The data are calculated for Cs_3C_{60} with $V_{C_{60}^{3-}} = 762 \text{ \AA}^3$ at 40 K. We assume the cRPA Coulomb interactions to be static, whose validity is substantiated in Section B in the Supplementary Materials. Inset: Frequency dependence of U_{eff} and U'_{eff} along the Matsubara frequency axis.

exotic s -wave superconductivity: (i) $U'_{eff} > U_{eff}$ and $J_{eff} < 0$ around $\omega = 0$ generate a singlet pair of electrons (leading to a Cooper pair) (19), which sit on the same orbital rather than on different orbitals as shown by $\langle n_{i\uparrow}n_{i\downarrow} \rangle > \langle n_{i\uparrow}n_{j\downarrow} \rangle$ in Fig. 4A. (ii) J_{eff} further enhances the pairing through a coherent tunneling of pairs between orbitals [the Suhl-Kondo mechanism (29, 30)].

As we have discussed above, these unusual multiorbital interactions are caused by phonons. In this sense, phonons are necessary to explain the superconductivity. However, strong electronic correlations also play a crucial role, marking a substantial difference from conventional phonon-driven superconductivity (17–19): The strong correlations heavily renormalize the electronic kinetic energy (from a bare value of ~ 0.5 eV) so that even the small difference (~ 33 to 37 meV) between U'_{eff} and U_{eff} is sufficient to bind the electrons into intraorbital pairs (19) [that is, it helps the mechanism (i)]. As a result, T_c increases with the correlation strength (see T_c versus $V_{C_{60}^{3-}}$ in Fig. 2A). This analysis clearly demonstrates that the superconductivity in alkali-doped fullerenes is the result of a synergy between electron-phonon interactions and electronic correlations (17, 18).

A peculiar low-spin Mott insulator

Also, the normal state displays remarkable consequences of the cooperative effect of the various interactions. Figure 4A shows the volume dependence of the intraorbital double occupancy D and the size S of the spin per molecule at $T = 40$ K. Here, we follow the metallic solution, expected to be stable in almost the entire coexistence region (25). In the Mott-insulating region with the Mott gap in the spectral function (Fig. 4B), S approaches $1/2$ (Fig. 4A), which is of the low-spin state, in agreement with the experimental observation (4–9). Another feature characteristic to the present Mott transition is the increase of D with the increase of the correlation strength, in sharp contrast with standard Mott transitions, in which D is drastically reduced.

This phenomenology also descends from $U_{eff} < U'_{eff}$ and $J_{eff} < 0$, which prefer onsite low-spin configurations with two electrons on one orbital (Fig. 4D). In the metallic phase, the electron hopping tends instead to make all the different local configurations equally likely (Fig. 4C) (19). As the correlation increases, the electrons gradually lose their kinetic energy, and hence, the six low-spin configurations ($\{n_1, n_2, n_3\} = \{2, 1, 0\}, \{0, 2, 1\}, \{1, 0, 2\}, \{2, 0, 1\}, \{1, 2, 0\}, \{0, 1, 2\}$) become the majority (Fig. 4C), which leads to the decrease (increase) of S (D). Eventually, in the Mott-insulating phase, these configurations become predominant.

Table 1. Material dependence of the static part of the phonon-mediated interactions. $U_{ph}(0)$, $U'_{ph}(0)$, and $J_{ph}(0)$ are the phonon-mediated onsite intraorbital, interorbital, and exchange interaction strengths between the t_{1u} electrons at $\omega = 0$ calculated with the cDFPT. The energy unit is eV. The numbers just after the material names denote the volume occupied per C_{60}^{3-} anion in \AA^3 .

	$U_{ph}(0)$	$U'_{ph}(0)$	$J_{ph}(0)$
K_3C_{60} (722)	-0.15	-0.053	-0.050
Rb_3C_{60} (750)	-0.14	-0.042	-0.051
Cs_3C_{60} (762)	-0.11	-0.013	-0.051
Cs_3C_{60} (784)	-0.12	-0.022	-0.051
Cs_3C_{60} (804)	-0.13	-0.031	-0.052

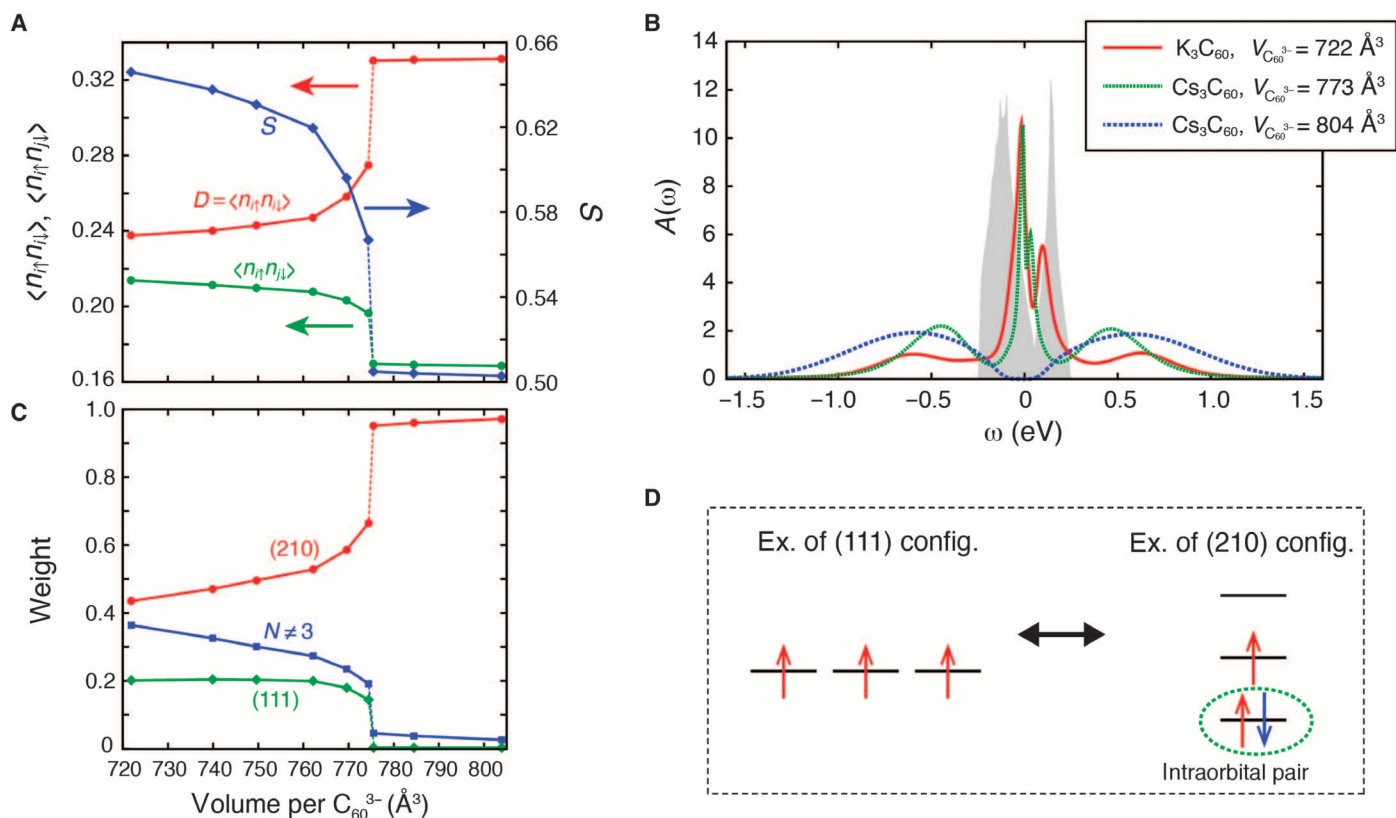


Fig. 4. Double occupancy, size of spin, weights of intramolecular configurations, spectral functions at 40 K, and schematic pictures of representative intramolecular configurations. (A) Volume dependence of the double-occupancy $D = \langle n_{\uparrow}n_{\downarrow} \rangle$ (red), the interorbital interspin correlation $\langle n_{\uparrow}n_{\downarrow} \rangle$ (green), and the size S of the spin per molecule (blue). (B) Spectral functions of several fcc A_3C_{60} systems at 40 K. For comparison, we show the DFT density of states for fcc K_3C_{60} ($V_{C_{60}^{3-}} = 722 \text{ \AA}^3$) as the shaded area. (C) Weights of several onsite configurations appearing in the quantum Monte Carlo simulations. (210) [(111)] generically denotes the configurations of $\{n_1, n_2, n_3\} = \{2, 1, 0\}$, $\{0, 2, 1\}$, $\{1, 0, 2\}$, $\{2, 0, 1\}$, $\{1, 2, 0\}$, $\{0, 1, 2\}$ [$\{n_1, n_2, n_3\} = \{1, 1, 1\}$], with n_i being the occupation of orbital i . $N \neq 3$ with $N = n_1 + n_2 + n_3$ denotes the configurations away from half filling. (D) Illustrative pictures for the (111) and (210) configurations. The up and down arrows indicate the up- and down-spin electrons, respectively.

Remarkably, the six (210) configurations, in each of which the orbital degeneracy is lifted (Fig. 4D), remain degenerate and no orbital ordering occurs. This unusual orbitally degenerate Mott state is consistent with the experimental observation of a dynamical Jahn-Teller effect (10).

DISCUSSION

We have carried out a fully ab initio study of the phase diagram of alkali-doped fullerides, in which all the interactions of a multiorbital Hubbard model coupled with phonons are computed from first principles with only the information on the atomic positions. The model is then solved by means of E-DMFT. We identify that a negative Hund's coupling arising from the electron-phonon interaction and the related condition $U_{\text{eff}} < U'_{\text{eff}}$ that favors intraorbital pairs (17, 18, 27, 28) underlie the existence of the superconducting state, its competition with the low-spin Mott state, and the whole phase diagram, which in turn remarkably reproduces the experimental observations.

This identifies a general condition under which a material can show a high-temperature electron-phonon superconducting phase that benefits from strong correlations (17), and suggests that a wider family of molecular conductors can exhibit a similar physics as long as an inverted Hund's exchange is stabilized by electron-phonon coupling. In

view of the accuracy demonstrated for A_3C_{60} , we can apply the methodology of this article to design other similar materials, possibly tailoring their properties to maximize the transition temperature.

MATERIALS AND METHODS

We apply the DFT + DMFT method (22) to fcc A_3C_{60} . We start from the global band structure (Fig. 1) obtained by the DFT (see Section A in the Supplementary Materials for the calculation conditions). Considering that the low-energy properties are governed by the isolated t_{1u} bands, we derive from first principles the lattice Hamiltonian (Eq. 1) for the t_{1u} electrons and the phonons.

As the basis for the lattice Hamiltonian, we construct the maximally localized Wannier orbitals (23) $\{\phi_{iR}\}$ from the t_{1u} bands. We calculate the transfer integrals by $t_{ij}(\mathbf{R}) = \langle \phi_{iR} | \mathcal{H}_{KS} | \phi_{j0} \rangle$ with the Kohn-Sham Hamiltonian \mathcal{H}_{KS} . $\mathcal{H}_{ij}^{(0)}(\mathbf{k})$ in Eq. 1 is the Fourier transform of $t_{ij}(\mathbf{R})$, which reproduces the original DFT band dispersion well (Fig. 1). The Coulomb interaction in the low-energy model incorporates the screening effects from the high-energy bands, whereas the screening processes within the t_{1u} bands are excluded to avoid duplication because the latter processes are taken into account when we solve the model. Such partially screened Coulomb parameters are calculated (26) with the

cRPA (31). Similarly, we calculate renormalized electron-phonon coupling $g_{ij}^y(\mathbf{k}, \mathbf{q})$ and phonon frequency $\omega_{\mathbf{q}\nu}$ by applying the recently developed cDFPT (24).

In the partition function for the lattice Hamiltonian (Eq. 1) written in the coherent state path integral formalism, we can integrate out the phonon degrees of freedom. This results in an electronic model with the additional electron-electron interaction (U_{ph} , U'_{ph} , and J_{ph}) mediated by phonons on top of the cRPA Coulomb interaction. The onsite phonon-mediated interaction $V_{ij,i'j'}$ (with $U_{\text{ph}} = V_{ii,ii}$, $U'_{\text{ph}} = V_{ii,ij}$, $J_{\text{ph}} = V_{ij,ij} = V_{ij,ji}$) is given, on the Matsubara axis, by (24):

$$V_{ij,i'j'}(i\Omega_n) = -\sum_{\mathbf{q}\nu} \tilde{g}_{ij}(\mathbf{q}, \nu) \frac{2\omega_{\mathbf{q}\nu}}{\Omega_n^2 + \omega_{\mathbf{q}\nu}^2} \tilde{g}_{i'j'}^*(\mathbf{q}, \nu),$$

where $\Omega_n = 2n\pi T$ is the bosonic Matsubara frequency and $\tilde{g}_{ij}(\mathbf{q}, \nu) = \frac{1}{N_{\mathbf{k}}} \sum_{\mathbf{k}} g_{ij}^y(\mathbf{k}, \mathbf{q})$ with the number $N_{\mathbf{k}}$ of \mathbf{k} -points. Here, the sum over the phonon branches runs from 1 to 189. In practice, we omit the lowest 9 branches [$\nu = 1$ to 9, which correspond to the acoustic modes, the librations, and the alkali-ion vibrations at the octahedral sites (20)]. This is justified because the coupling between these modes and the t_{1u} electrons is tiny (2).

We solve the derived lattice Hamiltonian by means of the E-DMFT (22), which maps the Hamiltonian (Eq. 1) onto a three-orbital single-impurity model embedded in noninteracting bath subject to self-consistent conditions. In the mapping, the E-DMFT incorporates the dynamical screening through the off-site interactions into the onsite interactions (U_V and U'_V) in a self-consistent way. To solve the impurity model, we use the continuous-time quantum Monte Carlo method based on the strong coupling expansion (32). Further detail can be found in Sections C and D in the Supplementary Materials.

The frequency dependence of U_V and U'_V in Fig. 3 is calculated with the Padé analytic continuation. We perform the analytic continuation onto $\omega + i\eta$ with $\eta = 0.01$ eV from the data along the Matsubara axis at 40 K for Cs_3C_{60} with $V_{C_{60}^3-} = 762 \text{ \AA}^3$. The spectral functions in Fig. 4B are calculated with the maximum entropy method.

SUPPLEMENTARY MATERIALS

Supplementary material for this article is available at <http://advances.sciencemag.org/cgi/content/full/1/77/e1500568/DC1>

Text (Sections A to F)

Fig. S1. Frequency dependence of partially screened Coulomb interactions for fcc Cs_3C_{60} with $V_{C_{60}^3-} = 762 \text{ \AA}^3$.

Fig. S2. Frequency dependence of the superconducting gap function at 10 K.

Table S1. Summary of input parameters for the E-DMFT calculations.

Table S2. Stability of superconducting (SC) solution at 10 K.

References (33–49)

REFERENCES AND NOTES

1. A. F. Hebard, M. J. Rosseinsky, R. C. Haddon, D. W. Murphy, S. H. Glarum, T. T. M. Palstra, A. P. Ramirez, A. R. Kortan, Superconductivity at 18 K in potassium-doped C_{60} . *Nature* **350**, 600–601 (1991).
2. O. Gunnarsson, *Alkali-Doped Fullerenes: Narrow-Band Solids with Unusual Properties* (World Scientific Publishing Co. Pte. Ltd., Singapore, 2004).
3. A. Y. Ganin, Y. Takabayashi, Y. Z. Khimyak, S. Margadonna, A. Tamai, M. J. Rosseinsky, K. Prassides, Bulk superconductivity at 38 K in a molecular system. *Nat. Mater.* **7**, 367–371 (2008).
4. Y. Takabayashi, A. Y. Ganin, P. Jeglič, D. Arčon, T. Takano, Y. Iwasa, Y. Ohishi, M. Takata, N. Takeshita, K. Prassides, M. J. Rosseinsky, The disorder-free non-BCS superconductor Cs_3C_{60} emerges from an antiferromagnetic insulator parent state. *Science* **323**, 1585–1590 (2009).

5. A. Y. Ganin, Y. Takabayashi, P. Jeglič, D. Arčon, A. Potočník, P. J. Baker, Y. Ohishi, M. T. McDonald, M. D. Tzirakis, A. McLennan, G. R. Darling, M. Takata, M. J. Rosseinsky, K. Prassides, Polymorphism control of superconductivity and magnetism in Cs_3C_{60} close to the Mott transition. *Nature* **466**, 221–225 (2010).
6. Y. Ihara, H. Alloul, P. Wzietek, D. Pontiroli, M. Mazzani, M. Riccò, NMR study of the Mott transitions to superconductivity in the two Cs_3C_{60} phases. *Phys. Rev. Lett.* **104**, 256402 (2010).
7. Y. Ihara, H. Alloul, P. Wzietek, D. Pontiroli, M. Mazzani, M. Riccò, Spin dynamics at the Mott transition and in the metallic state of the Cs_3C_{60} superconducting phases. *Europhys. Lett.* **94**, 37007 (2011).
8. P. Wzietek, T. Mito, H. Alloul, D. Pontiroli, M. Aramini, M. Riccò, NMR study of the superconducting gap variation near the Mott transition in Cs_3C_{60} . *Phys. Rev. Lett.* **112**, 066401 (2014).
9. R. H. Zadik, Y. Takabayashi, G. Klupp, R. H. Colman, A. Y. Ganin, A. Potočník, P. Jeglič, D. Arčon, P. Matus, K. Kamarás, Y. Kasahara, Y. Iwasa, A. N. Fitch, Y. Ohishi, G. Garbarino, K. Kato, M. J. Rosseinsky, K. Prassides, Optimized unconventional superconductivity in a molecular Jahn-Teller metal. *Sci. Adv.* **1**, e1500059 (2015).
10. G. Klupp, P. Matus, K. Kamarás, A. Y. Ganin, A. McLennan, M. J. Rosseinsky, Y. Takabayashi, M. T. McDonald, K. Prassides, Dynamic Jahn-Teller effect in the parent insulating state of the molecular superconductor Cs_3C_{60} . *Nat. Commun.* **3**, 912 (2012).
11. C. M. Varma, J. Zaanen, K. Raghavachari, Superconductivity in the fullerenes. *Science* **254**, 989–992 (1991).
12. M. Schluter, M. Lannoo, M. Needels, G. A. Baraff, D. Tománek, Electron-phonon coupling and superconductivity in alkali-intercalated C_{60} solid. *Phys. Rev. Lett.* **68**, 526–529 (1992).
13. I. I. Mazin, O. V. Dolgov, A. Golubov, S. V. Shulga, Strong-coupling effects in alkali-metal-doped C_{60} . *Phys. Rev. B Condens. Matter* **47**, 538–541 (1993).
14. F. C. Zhang, M. Ogata, T. M. Rice, Attractive interaction and superconductivity for K_3C_{60} . *Phys. Rev. Lett.* **67**, 3452–3455 (1991).
15. S. Chakravarty, M. P. Gelfand, S. Kivelson, Electronic correlation effects and superconductivity in doped fullerenes. *Science* **254**, 970–974 (1991).
16. S. Suzuki, S. Okada, K. Nakano, Theoretical study on the superconductivity induced by the dynamic Jahn-Teller effect in alkali-metal-doped C_{60} . *J. Phys. Soc. Jpn.* **69**, 2615–2622 (2000).
17. M. Capone, M. Fabrizio, C. Castellani, E. Tosatti, Strongly correlated superconductivity. *Science* **296**, 2364–2366 (2002).
18. M. Capone, M. Fabrizio, C. Castellani, E. Tosatti, *Colloquium: Modeling the unconventional superconducting properties of expanded A_3C_{60} fullerides*. *Rev. Mod. Phys.* **81**, 943–958 (2009).
19. J. E. Han, O. Gunnarsson, V. H. Crespi, Strong superconductivity with local Jahn-Teller phonons in C_{60} solids. *Phys. Rev. Lett.* **90**, 167006 (2003).
20. R. Akashi, R. Arita, Nonempirical study of superconductivity in alkali-doped fullerides based on density functional theory for superconductors. *Phys. Rev. B* **88**, 054510 (2013).
21. J. L. Janssen, M. Côté, S. G. Louie, M. L. Cohen, Electron-phonon coupling in C_{60} using hybrid functionals. *Phys. Rev. B Condens. Matter* **81**, 073106 (2010).
22. G. Kotliar, S. Y. Savrasov, K. Haule, V. S. Oudovenko, O. Parcollet, C. A. Marianetti, Electronic structure calculations with dynamical mean-field theory. *Rev. Mod. Phys.* **78**, 865–951 (2006).
23. N. Marzari, D. Vanderbilt, Maximally localized generalized Wannier functions for composite energy bands. *Phys. Rev. B Condens. Matter* **56**, 12847–12865 (1997).
24. Y. Nomura, K. Nakamura, R. Arita, Effect of electron-phonon interactions on orbital fluctuations in iron-based superconductors. *Phys. Rev. Lett.* **112**, 027002 (2014).
25. K. Inaba, A. Koga, S.-i. Suga, N. Kawakami, Finite-temperature Mott transitions in the multi-orbital Hubbard model. *Phys. Rev. B Condens. Matter* **72**, 085112 (2005).
26. Y. Nomura, K. Nakamura, R. Arita, *Ab initio* derivation of electronic low-energy models for C_{60} and aromatic compounds. *Phys. Rev. B Condens. Matter* **85**, 155452 (2012).
27. M. Capone, M. Fabrizio, E. Tosatti, Direct transition between a singlet Mott insulator and a superconductor. *Phys. Rev. Lett.* **86**, 5361–5364 (2001).
28. M. Capone, M. Fabrizio, C. Castellani, E. Tosatti, Strongly correlated superconductivity and pseudogap phase near a multiband Mott insulator. *Phys. Rev. Lett.* **93**, 047001 (2004).
29. H. Suhl, B. T. Matthias, L. R. Walker, Bardeen-Cooper-Schrieffer theory of superconductivity in the case of overlapping bands. *Phys. Rev. Lett.* **3**, 552–554 (1959).
30. J. Kondo, Superconductivity in transition metals. *Prog. Theor. Phys.* **29**, 1–9 (1963).
31. F. Aryasetiawan, M. Imada, A. Georges, G. Kotliar, S. Biermann, A. I. Lichtenstein, Frequency-dependent local interactions and low-energy effective models from electronic structure calculations. *Phys. Rev. B Condens. Matter* **70**, 195104 (2004).
32. P. Werner, A. Comanac, L. de' Medici, M. Troyer, A. J. Millis, Continuous-time solver for quantum impurity models. *Phys. Rev. Lett.* **97**, 076405 (2006).
33. P. Giannozzi, S. Baroni, N. Bonini, M. Calandra, R. Car, C. Cavazzoni, D. Ceresoli, G. L. Chiarotti, M. Cococcioni, I. Dabo, A. D. Corso, S. de Gironcoli, S. Fabris, G. Fratesi, R. Gebauer, U. Gerstmann, C. Gougousis, A. Kokalj, M. Lazzeri, L. Martin-Samos, N. Marzari, F. Mauri, R. Mazzarello, S. Paolini, A. Pasquarello, L. Paulatto, C. Sbraccia, S. Scandolo, G. Sclauzero, A. P. Seitsonen, A. Smogunov,

- P. Umari, R. M. Wentzcovitch, QUANTUM ESPRESSO: A modular and open-source software project for quantum simulations of materials. *J. Phys. Condens. Matter* **21**, 395502 (2009).
34. J. P. Perdew, A. Zunger, Self-interaction correction to density-functional approximations for many-electron systems. *Phys. Rev. B* **23**, 5048–5079 (1981).
35. N. Troullier, J. L. Martins, Efficient pseudopotentials for plane-wave calculations. *Phys. Rev. B* **43**, 1993–2006 (1991).
36. L. Kleinman, D. M. Bylander, Efficacious form for model pseudopotentials. *Phys. Rev. Lett.* **48**, 1425–1428 (1982).
37. S. G. Louie, S. Froyen, M. L. Cohen, Nonlinear ionic pseudopotentials in spin-density-functional calculations. *Phys. Rev. B Condens. Matter* **26**, 1738–1742 (1982).
38. D. D. Koelling, B. N. Harmon, A technique for relativistic spin-polarised calculations. *J. Phys. C Solid State Phys.* **10**, 3107–3114 (1977).
39. T. Fujiwara, S. Yamamoto, Y. Ishii, Generalization of the iterative perturbation theory and metal-insulator transition in multi-orbital Hubbard bands. *J. Phys. Soc. Jpn.* **72**, 777–780 (2003).
40. Y. Nohara, S. Yamamoto, T. Fujiwara, Electronic structure of perovskite-type transition metal oxides LaMO_3 ($M = \text{Ti} \sim \text{Cu}$) by U + GW approximation. *Phys. Rev. B Condens. Matter* **79**, 195110 (2009).
41. M. S. Golden, M. Knupfer, J. Fink, J. F. Armbuster, T. R. Cummins, H. A. Romberg, M. Roth, M. Sing, M. Schmidt, E. Sohmen, The electronic structure of fullerenes and fullerene compounds from high-energy spectroscopy. *J. Phys. Condens. Matter* **7**, 8219–8247 (1995).
42. A. M. Sengupta, A. Georges, Non-Fermi-liquid behavior near a $T=0$ spin-glass transition. *Phys. Rev. B Condens. Matter* **52**, 10295–10302 (1995).
43. Q. Si, J. L. Smith, Kosterlitz-Thouless transition and short range spatial correlations in an extended Hubbard model. *Phys. Rev. Lett.* **77**, 3391–3394 (1996).
44. P. Sun, G. Kotliar, Extended dynamical mean-field theory and GW method. *Phys. Rev. B Condens. Matter* **66**, 085120 (2002).
45. T. Ayrál, S. Biermann, P. Werner, Screening and nonlocal correlations in the extended Hubbard model from self-consistent combined GW and dynamical mean field theory. *Phys. Rev. B Condens. Matter* **87**, 125149 (2013).
46. I. G. Lang, Yu. A. Firsov, Kinetic theory of semiconductors with low mobility. *Sov. J. Exp. Theor. Phys.* **16**, 1301 (1963).
47. P. Werner, A. J. Millis, Efficient dynamical mean field simulation of the Holstein-Hubbard model. *Phys. Rev. Lett.* **99**, 146404 (2007).
48. K. Steiner, Y. Nomura, P. Werner, Double-expansion impurity solver for multiorbital models with dynamically screened U and J , arXiv:1506.01173.
49. A. Koga, P. Werner, Superconductivity in the two-band Hubbard model. *Phys. Rev. B Condens. Matter* **91**, 085108 (2015).

Acknowledgments: We would like to thank K. Nakamura for valuable comments on the manuscript, and Y. Iwasa and Y. Kasahara for fruitful discussions and for providing us with the experimental phase diagram. We acknowledge useful discussions with P. Werner, T. Ayrál, Y. Murakami, H. Shinaoka, N. Parragh, G. Sangiovanni, M. Imada, A. Oshiyama, A. Fujimori, P. Wzietek, H. Alloul, M. Fabrizio, E. Tosatti, and G. Giovannetti. Some of the calculations were performed at the Supercomputer Center, The Institute for Solid State Physics (ISSP), University of Tokyo. **Funding:** Y.N. is supported by Grant-in-Aid for JSPS Fellows (no. 12J08652) from Japan Society for the Promotion of Science (JSPS), Japan. S.S. is supported by Grant-in-Aid for Scientific Research (no. 26800179), from JSPS Japan. M.C. is supported by FP7/European Research Council (ERC) through the Starting Grant SUPERBAD (grant agreement no. 240524) and by the EU-Japan Project LEMSUPER (grant agreement no. 283214). **Author contributions:** Y.N. performed the calculations. All the authors discussed the calculated results and wrote the manuscript. M.C. and R.A. conceived the project. **Competing interests:** The authors declare that they have no competing interests.

Submitted 5 May 2015

Accepted 15 July 2015

Published 21 August 2015

10.1126/sciadv.1500568

Citation: Y. Nomura, S. Sakai, M. Capone, R. Arita, Unified understanding of superconductivity and Mott transition in alkali-doped fullerenes from first principles. *Sci. Adv.* **1**, e1500568 (2015).

This article is published under a Creative Commons license. The specific license under which this article is published is noted on the first page.

For articles published under [CC BY](#) licenses, you may freely distribute, adapt, or reuse the article, including for commercial purposes, provided you give proper attribution.

For articles published under [CC BY-NC](#) licenses, you may distribute, adapt, or reuse the article for non-commercial purposes. Commercial use requires prior permission from the American Association for the Advancement of Science (AAAS). You may request permission by clicking [here](#).

The following resources related to this article are available online at <http://advances.sciencemag.org>. (This information is current as of May 24, 2017):

Updated information and services, including high-resolution figures, can be found in the online version of this article at:

<http://advances.sciencemag.org/content/1/7/e1500568.full>

Supporting Online Material can be found at:

<http://advances.sciencemag.org/content/suppl/2015/08/20/1.7.e1500568.DC1>

This article **cites 47 articles**, 6 of which you can access for free at:

<http://advances.sciencemag.org/content/1/7/e1500568#BIBL>

Science Advances (ISSN 2375-2548) publishes new articles weekly. The journal is published by the American Association for the Advancement of Science (AAAS), 1200 New York Avenue NW, Washington, DC 20005. Copyright is held by the Authors unless stated otherwise. AAAS is the exclusive licensee. The title *Science Advances* is a registered trademark of AAAS